Materials Transactions, Vol. 64, No. 8 (2023) pp. 1974 to 1981

Electrodeposition of Cobalt from LiCl-Based Highly Concentrated Aqueous Solution: Crystal Phase and Hydrogen Content

Ryutaro Miura[1,*1], Tomoya Hashimoto[2,*2], Kazuhiro Fukami[1], Naoki Fukumuro[2], Shinji Yae[2] and Kuniaki Murase[1,*3]

[1]*Department of Materials Science and Engineering, Kyoto University, Kyoto 606-8501, Japan*
[2]*Graduate School of Engineering, University of Hyogo, Himeji 671-2280, Japan*

The relationship between the crystal phase and absorbed hydrogen in cobalt electrodeposited from a LiCl-based highly concentrated (HC) aqueous solution was investigated using X-ray diffraction and thermal desorption spectroscopy. We expected that the use of an HC solution would enable the electrodeposition of cobalt without hydrogen evolution and the concomitant hydrogen absorption. The current efficiency of cobalt deposition was more than 99% at potentials above −0.8 V vs. Ag/AgCl, indicating that hydrogen evolution is really suppressed, but the electrodeposited cobalt accompanied the fcc phase irrespective of the deposition temperature. Moreover, electrodeposited cobalt contained a large amount of hydrogen despite the high current efficiency. The hydrogen content of cobalt obtained at 100°C was approximately 10% of that obtained at room temperature; however, the fcc phase was still co-deposited, suggesting that factors other than hydrogen could be responsible for fcc-Co formation. The reason for hydrogen inclusion from the HC solution is discussed in terms of the hydrogen reduction mechanism.
[doi:10.2320/matertrans.MT-M2023014]

(Received February 1, 2023; Accepted May 22, 2023; Published June 9, 2023)

Keywords: *cobalt electrodeposition, aqueous solution, hydrate melt, hydrogen evolution, hydrogen co-deposition, crystal phase*

1. Introduction

Elemental cobalt (Co) changes its crystalline form with a boundary at approximately 420°C, wherein at lower temperatures the hcp structure is stable and at higher temperatures the fcc phase is stable.[1)] Elemental cobalt or Co metal is usually obtained by electrodeposition from an aqueous solution containing Co^{2+} ions. Although such aqueous electrodeposition is carried out at room temperature, the high-temperature fcc phase sometimes appears in the electrodeposited Co.[2,3)] If the fcc phase, which is metastable at lower temperatures, is formed by electrodeposition and then gradually transforms into the stable hcp phase by aging, changes in the physical properties (strength, magnetism, conductivity, etc.) could impede the use of cobalt metal as a material. Elemental cobalt has never been applied as a material; however, it has recently become a candidate material for ultrafine wiring.[4,5)]

It is known that electrodeposition of the fcc Co occurs under conditions such as low pH, high cathodic deposition overvoltage, and high cathodic current density,[2,3,6–9)] where a large amount of hydrogen evolution takes place as a side reaction. Cobalt has a more negative electrode potential than hydrogen evolution; therefore, cobalt electrodeposition from aqueous solutions is accompanied by hydrogen evolution. This suggests that hydrogen evolution, or the co-deposition of hydrogen, is relevant to the electrodeposited cobalt phase. To examine the effect of hydrogen on cobalt electrodeposits, a comparison of cobalt electrodeposition using aqueous solutions reported in previous studies with that using an electrolyte *without* hydrogen evolution would be helpful. Hydrogen evolution during metal electrodeposition can also cause other problems, such as hydrogen embrittlement[10)] and the co-deposition of hydroxides due to a local increase in pH near the cathodes.

In the case of cobalt and other metal electrodepositions, one approach to exclude the effect of hydrogen is to use aprotic nonaqueous solutions in which hydrogen evolution does not occur. For example, some ionic liquids and deep eutectic solutions (DES) do not generate hydrogen over a wide potential range. However, elemental cobalt electrodeposited from ionic liquids sometimes shows poor crystallinity,[11)] which makes it difficult to discuss the crystal phase. Moreover, ionic liquids are generally expensive and cannot be handled in air; such properties of ionic liquids are not viable for the industrial electrodeposition of metals. In the case of choline-urea DES —a well-known DES system— in addition to poor crystallinity,[12,13)] our preliminary experiments have shown that solution decomposition occurs at the electrodeposition potential of cobalt.

Recently a series of highly concentrated (HC) aqueous solutions, also known as water-in-salt electrolytes (WiSE) or hydrate melts, have been recognized as "solvents" that can suppress hydrogen evolution.[14,15)] The suppression of water splitting in HC solutions is due to a decrease the activity of free water in the presence of high concentrated indifferent salt(s).[16–18)] Taking advantage of this unique characteristic, the HC aqueous solution has been studied as an electrolyte for lithium-ion batteries,[19,20)] zinc-air batteries,[21,22)] and electroplating solutions.[23,24)] In particular, crystalline chromium coating was successfully electrodeposited from a trivalent chromium bath with high current efficiency.[25)]

In the present study, we selected a LiCl-based HC aqueous solution as a medium for cobalt electrodeposition, to investigate whether hydrogen evolution could be suppressed and if the resulting crystal phase would be an hcp or fcc close-packed lattice.

*[1]Graduate Student, Kyoto University
*[2]Graduate Student, University of Hyogo
*[3]Corresponding author, E-mail: murase.kuniaki.2n@kyoto-u.ac.jp

2. Experimental

2.1 Electrochemical measurements

All aqueous solutions were prepared with reagent-grade chemicals purchased from Nacalai Tesque, except for $CoCl_2 \cdot 6H_2O$ (Fujifilm Wako) and deionized water (resistivity 18 MΩ cm) obtained using a Milli-Q system. Aqueous solutions with H_2O/LiCl molar ratios (n) of 3, 9, 55, and 555 containing 0.3 mol dm^{-3} $CoCl_2 \cdot 6H_2O$ or 10 mmol dm^{-3} HCl were used as electrolytes. Here, the solutions with $n =$ 3 and 9 fall into the category of HC solutions. All the electrochemical measurements were performed using a three-electrode cell with a potentiostat (Bio-Logic Science Instruments, SP-300). Linear sweep voltammetry (LSV) was performed using a Pt disk electrode as the working electrode, a glassy carbon sheet as the counter electrode, and Ag/AgCl in 3.33 mol dm^{-3} KCl aqueous solution as the reference electrode. Hydrodynamic voltammetry was performed to determine the diffusion coefficients of Co^{2+} and H^+ in the electrolytes. The electrolytes measured were the $n = 3$ solution containing 0.3 mol dm^{-3} $CoCl_2$ or 10 mmol dm^{-3} HCl. A Pt rotating disk electrode (RDE; diameter, 5 mm) was used as the working electrode, and the counter and reference electrodes were the same as those used in the above-described LSV measurements. A rotating electrode system (Hokuto Denko, Dynamic Electrode HR-201) was employed to control the rotation rate.

2.2 Electrodeposition of cobalt

The HC solution ($n = 3$) containing 0.3 mol dm^{-3} $CoCl_2$ was used for the electrodeposition of cobalt. The pH of the as-prepared solution was 4.0. A dilute aqueous solution containing only 0.3 mol dm^{-3} $CoCl_2$, without LiCl, was also used for comparison. A series of potentiostatic electrodepositions was performed with a tungsten (W) sheet as the working electrode, a Co sheet as the counter electrode, and an Ag/AgCl in 3.33 mol dm^{-3} KCl aqueous solution as the reference electrode. The use of bcc phase W substrate facilitated the recognition of the X-ray diffraction lines of the resulting hcp and fcc Co. For the HC solution ($n = 3$), six different electrodeposition potentials, −0.65, −0.70, −0.75, −0.80, −0.85, and −0.90 V vs. Ag/AgCl were investigated at room temperature. Another series of potentiostatic depositions was carried out at 50, 75, and 100°C to examine the effect of the solution temperature. In this case, the applied potential of each electrodeposition was unified at −0.4 V vs. immersion potential of Co to each solution. For comparison, electrodeposition from the dilute solution was also performed at −0.4 V vs. the immersion potential of Co at room temperature. Note that the −0.4 V vs. the immersion potential of Co in HC solutions at room temperature corresponds to −0.75 V vs. Ag/AgCl. The total electric charge was unified to 10 C cm^{-2} for all electrodeposition runs, wherein the charge corresponds to a Co thickness of approximately 3.4 μm if there is no side reaction.

The current efficiency was calculated from the above-mentioned electric charge (10 C cm^{-2}) and the amount of deposited Co using Faraday's law. The amount of Co was determined from the weight, measured by a microbalance (Mettler Toledo), and the charge obtained by the anode stripping (AS) method. In the latter case, the deposits after each electrodeposition were dissolved at −0.2 V vs. Ag/AgCl.

2.3 Characterization

Viscosities of the solutions were obtained at room temperature using a viscometer (EMS-1000, Kyoto Electronics Manufacturing Co., Ltd.). Solution densities were calculated by using the measured values of weight and volume at room temperature. Kinematic viscosities were calculated by dividing the viscosities by the solution densities.

X-ray diffraction (XRD) was performed to determine the crystal phase of the electrodeposits using a Rigaku RINT-2200 system with Cu-Kα radiation at 40 kV and 30 mA. X-ray photoelectron spectroscopy (XPS) measurements were performed using a JEOL JPS-9010TRX instrument with monochromatic Mg-Kα radiation.

The hydrogen content of the electrodeposits was determined using thermal desorption spectroscopy (TDS) apparatus equipped with a quadrupole mass spectrometer (M-201QA-TDM, Canon Anelva) to detect the hydrogen desorbed from each sample. Each sample was placed in a quartz tube sealed at one end and kept at a pressure below 10^{-5} Pa, and TDS was performed in the temperature range of 300–1000 K with a temperature increase rate of 5 K min^{-1}. Quantification of hydrogen in the cobalt electrodeposits was achieved using a standard curve prepared with magnesium hydride (MgH_2) as a standard sample.[26)]

3. Results and Discussions

3.1 Electrochemical measurements

Prior to the electrodeposition of Co, the polarization behavior of the solutions was investigated. Figure 1(a) shows a set of cathodic linear sweep voltammograms for aqueous solutions containing four different concentrations of LiCl and 0.3 mol dm^{-3} $CoCl_2$. The first reduction wave rising from −0.6 V corresponds to the reduction of Co^{2+}: $Co^{2+} + 2e^- =$ Co. After the first wave, the current decreased once to provide a low-current region and then increased again. The low-current region well-corresponds with the limiting currents for the reduction of Co^{2+}. Despite the same concentration of Co^{2+}, the limiting current decreased with the decrease in n, because the viscosity of the solution increased with decreasing n. The second reduction current observed below −1.0 V is the direct reduction of water: $2H_2O + 2e^- = H_2 + 2OH^-$. We predicted that another hydrogen evolution by the reduction of protons, $2H^+ + 2e^- = H_2$, should occur in the potential range overlapping with that of the Co electrodeposition; however, its current was unclear (Fig. 1(a)). Therefore, we performed another set of voltammetry measurements using four different solutions containing 10 mmol dm^{-3} HCl instead of 0.3 mol dm^{-3} $CoCl_2$ (Fig. 1(b)). The onset of the hydrogen evolution from protons was found in the potential range of −0.1 to −0.3 V. Despite the same HCl concentration, the current of hydrogen evolution by proton reduction was also significantly suppressed with decreasing n. Specifically, the current for the $n = 3$ solution with highly concentrated LiCl was one-eighth

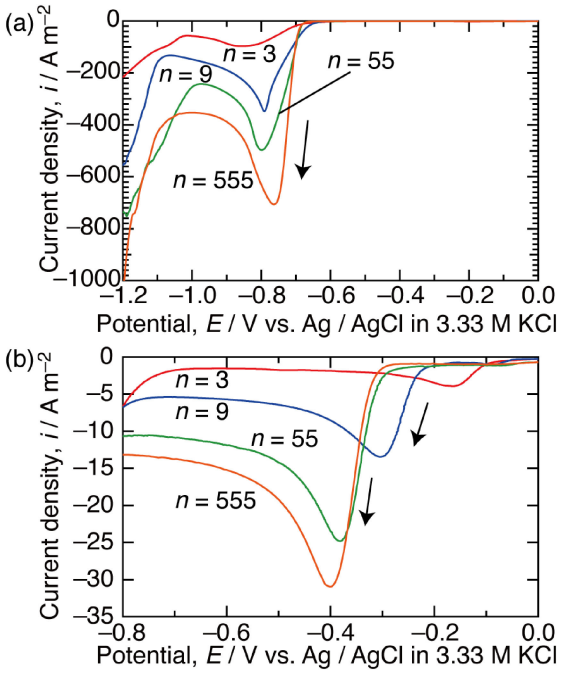

Fig. 1 Linear sweep voltammograms for solutions with H_2O/LiCl molar ratios (n) of 3, 9, 55, and 555 containing (a) 0.3 mol dm^{-3} $CoCl_2$ and (b) 10 mmol dm^{-3} HCl.

of that of $n = 555$ with 0.1 mol dm^{-3} LiCl, which is considered a *standard* concentration.

To discuss the transport properties of Co^{2+} and H^+ ions quantitatively, cathodic hydrodynamic voltammetry using RDE was carried out for $n = 3$ solutions with 0.3 mol dm^{-3} $CoCl_2$ or 10 mmol dm^{-3} HCl as shown in Figs. 2(a) and 2(b), respectively. Here, the relationship between the limiting current density i_L and angular velocity ω of the rotating electrode follows the Levich equation, $i_L = -0.62 mFD^{2/3}\nu^{-1/6}c\omega^{1/2}$, where D is the diffusion coefficient of the ions, ν is the kinematic viscosity of the solution, c is the concentration of the ions (i.e., the active reactant), F is the Faraday constant, and m is the number of electrons transferred in the reaction. The viscosity (μ) and the density (d) of $n = 3$ solutions with 0.3 mol dm^{-3} $CoCl_2$ and 10 mmol dm^{-3} HCl were 14.7 and 13.6 mPa s, 1.29 and 1.28 g cm^{-3}, respectively. Then, ν of $n = 3$ solutions with 0.3 mol dm^{-3} $CoCl_2$ and 10 mmol dm^{-3} HCl were calculated to be 0.114 and 0.106 cm^2 s^{-1}, respectively. Based on the Levich equation, the $|i_L|$ vs. $\omega^{1/2}$ plots (Levich plots) shown in Figs. 2(c) and (d) show the diffusion coefficients of the Co^{2+} ions and protons, respectively, as the values calculated from each slope. Table 1 summarizes the resulting coefficients together with those for the dilute aqueous solution systems.[27] In the HC solution, the diffusion coefficients for both Co^{2+} ($D_{Co^{2+}}$) and H^+ (D_{H^+}) decreased by one or two orders of magnitude compared with those of the dilute solution, owing to the increase in viscosity. The $D_{H^+}/D_{Co^{2+}}$ ratio decreased from 12.7 to 1.06, indicating that proton diffusion was more suppressed. This phenomenon is caused

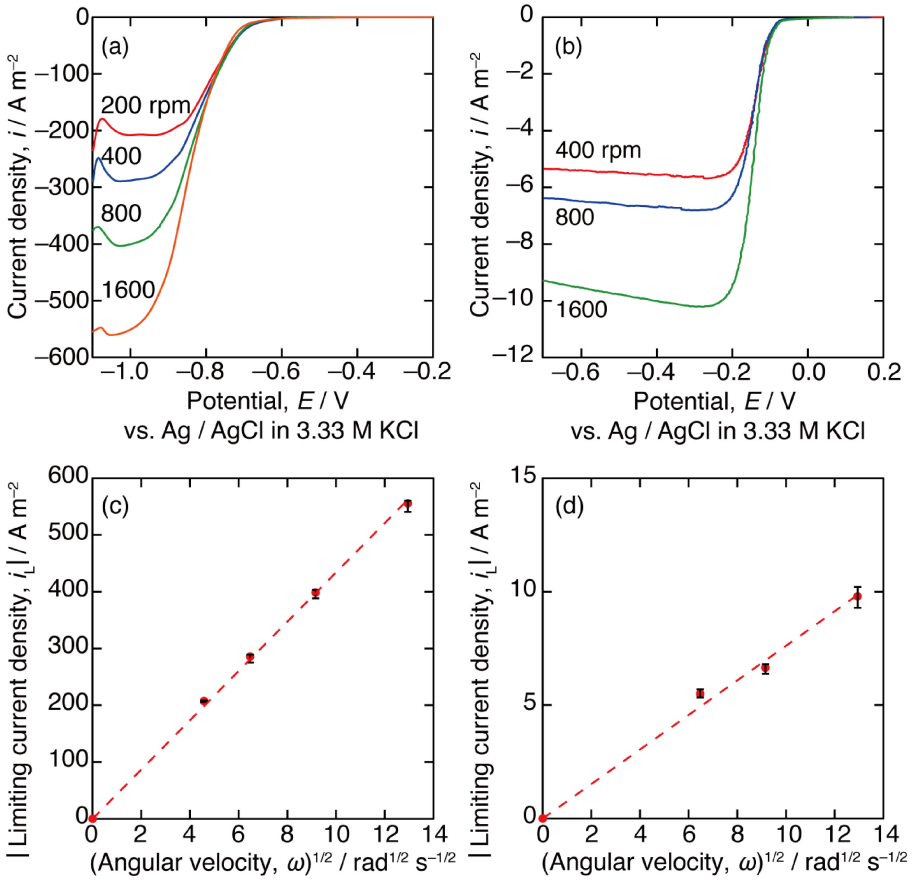

Fig. 2 Cathodic hydrodynamic voltammograms for HC solution ($n = 3$) containing (a) 0.3 mol dm^{-3} $CoCl_2$ and (b) 10 mmol dm^{-3} HCl. Working electrode was Pt RDE with four different values of the rotating rate ω. Relationship between the limiting current density $|i_L|$ and $\omega^{1/2}$ (Levich plot) for (c) Co electrodeposition and (d) hydrogen evolution is obtained from the data of (a) and (b), respectively.

Table 1 Proton and Co^{2+} diffusion coefficients and the ratios between the proton and Co^{2+} diffusion coefficients in the HC ($n = 3$) and dilute solutions.

	D_{H^+}	$D_{Co^{2+}}$	$D_{H^+}/D_{Co^{2+}}$	Ref.
$n = 3$	8.2×10^{-7}	7.7×10^{-7}	1.06	This study
Dilute	9.3×10^{-5}	0.7×10^{-5}	12.7	27

by the disappearance of the Grotthuss mechanism, a fast proton hopping mechanism, in HC aqueous solutions where free water molecules are deficient.[28] We expected that such suppression of hydrogen evolution in the HC LiCl solution would make it possible to electrodeposit Co under a high current efficiency, even though the solution is aqueous.

3.2 Potentiostatic electrodeposition of cobalt

Based on the above voltammograms, we selected six potentials between −0.65 to −0.90 V to electrodeposit Co. The current efficiencies for the six potentiostatic Co depositions obtained using the two methods (Experimental section) are listed in Table 2. The current efficiencies in the HC solution ($n = 3$) determined by the AS method were almost 100% at −0.65, −0.70, and −0.75 V. Even at −0.80 V, the current efficiency exceeded 97%, indicating that the hydrogen evolution in HC solution is almost suppressed at potentials above −0.8 V. However, at −0.80 V or lower potential, the efficiency determined by the weight exceeded 100%. The inconsistency could be caused by the formation of cobalt(II) oxides and/or hydroxides near the cathode because of the increase in pH due to hydrogen evolution, while XRD measurements did not detect the phases (Fig. 3). The buffer capacity of HC solutions is generally lower than that of ordinal aqueous solutions,[29] resulting in the ease of formation of oxides/hydroxides. Therefore, we believe that the current efficiency data obtained using the AS method, which decreased monotonically with increasing cathodic polarization, were more reliable. In any case, we can conclude that the use of an HC solution is an effective method to avoid hydrogen evolution during the electrodeposition of Co. Note that the Co electrodeposition efficiencies at −0.4 V (vs. Co immersion potential) in the HC solution at elevated temperatures are 98.2% (50°C), 99.9% (75°C), and 100.6% (100°C) and the efficiency in the dilute solution is 59.9%, as obtained by the AS method.

Figure 3(a) shows the XRD patterns of the electrodeposits obtained from the HC ($n = 3$) and dilute solutions at room temperature. Electrodeposition from the HC ($n = 3$) solution was performed at six different potentials. Diffraction peaks corresponding to hcp cobalt were observed at $2\theta = 41.6°$ (100), 44.4° (002), 47.4° (101), 75.8° (110), and 92.3° (112) for the electrodeposits obtained from the dilute solutions. Here, no clear diffraction peaks due to the fcc phase were observed. In contrast, in the electrodeposits obtained at −0.65 to −0.8 V from the HC solution, the 200 diffraction peak corresponding to fcc cobalt was observed at 51.5° in addition to the diffraction peaks of hcp-Co, indicating the co-deposition of fcc-Co. It was believed that the co-deposition of the fcc phase from aqueous solutions requires a large amount of simultaneous hydrogen evolution.[2] Our results, however, indicate that remarkable hydrogen evolution is not always necessary for the co-deposition of the fcc phase in the case of cobalt electrodeposition from HC solution. Figure 3(b) shows the XRD patterns of cobalt electrodeposited at higher temperatures, 50, 75, and 100°C, which reveal that co-deposition of fcc-Co occurred even at elevated temperatures. In general, electrodeposition at elevated temperatures tends to produce thermodynamically stable phases, i.e., the hcp phase in this case. In fact, for the electrodeposition of cobalt from conventional dilute aqueous solutions, it has been reported that metastable phases (i.e., fcc) are less likely to be appeared at elevated temperatures.[30,31] Thus, our results showing that a metastable phase was electrodeposited even at higher temperatures is quite unique.

The XPS quantitative analysis results for cobalt obtained at room temperature from the HC solutions ($n = 3$) by constant potential electrodeposition at −0.75 V are listed in Table 3. Lithium (Li) and chlorine (Cl), the main components of the electrolyte, were not detected in the cobalt interior. Although hydroxides were detected at the surface due to native oxidation, 99% of the interior cobalt was metallic. Note that the sputtered depth by Ar^+ sputtering time of 1500 s corresponds to 100 nm in terms of SiO_2. Therefore, it was confirmed that the electrodeposit was almost pure cobalt without oxide/hydroxide.

The amount of hydrogen in the electrodeposited cobalt was determined using TDS measurements. Figure 4(a) compares the TDS spectra of cobalt electrodeposited at a polarization of −0.4 V (vs. immersion potential of Co) from the HC and dilute solutions at room temperature. Figure 4(b) shows the TDS spectra of cobalt electrodeposited at the same potential from the HC solution at high temperatures. For the electrodeposits from HC solution at room temperature, 50, and 75°C, a set of hydrogen desorption peaks were observed at several different temperatures between 300 and 1000 K.

Regarding the state of hydrogen in the cobalt electrodeposits, a peak at $T = 350$ K, which was observed in the

Table 2 Current efficiencies of cobalt electrodeposition from the HC ($n = 3$) and dilute solutions at room temperature. In the dilute solution, electrodeposition was performed at −0.4 V vs. immersion potential of Co.

Method	Current efficiency / %						
	Potential, E / V vs. Ag/AgCl in 3.33 mol dm^{-3} KCl						
	−0.65	−0.70	−0.75	−0.80	−0.85	−0.90	Dilute solution
Weight	100	100	100	100	102	110	—
AS	100.1	100.4	99.3	97.8	96.8	94.7	59.9

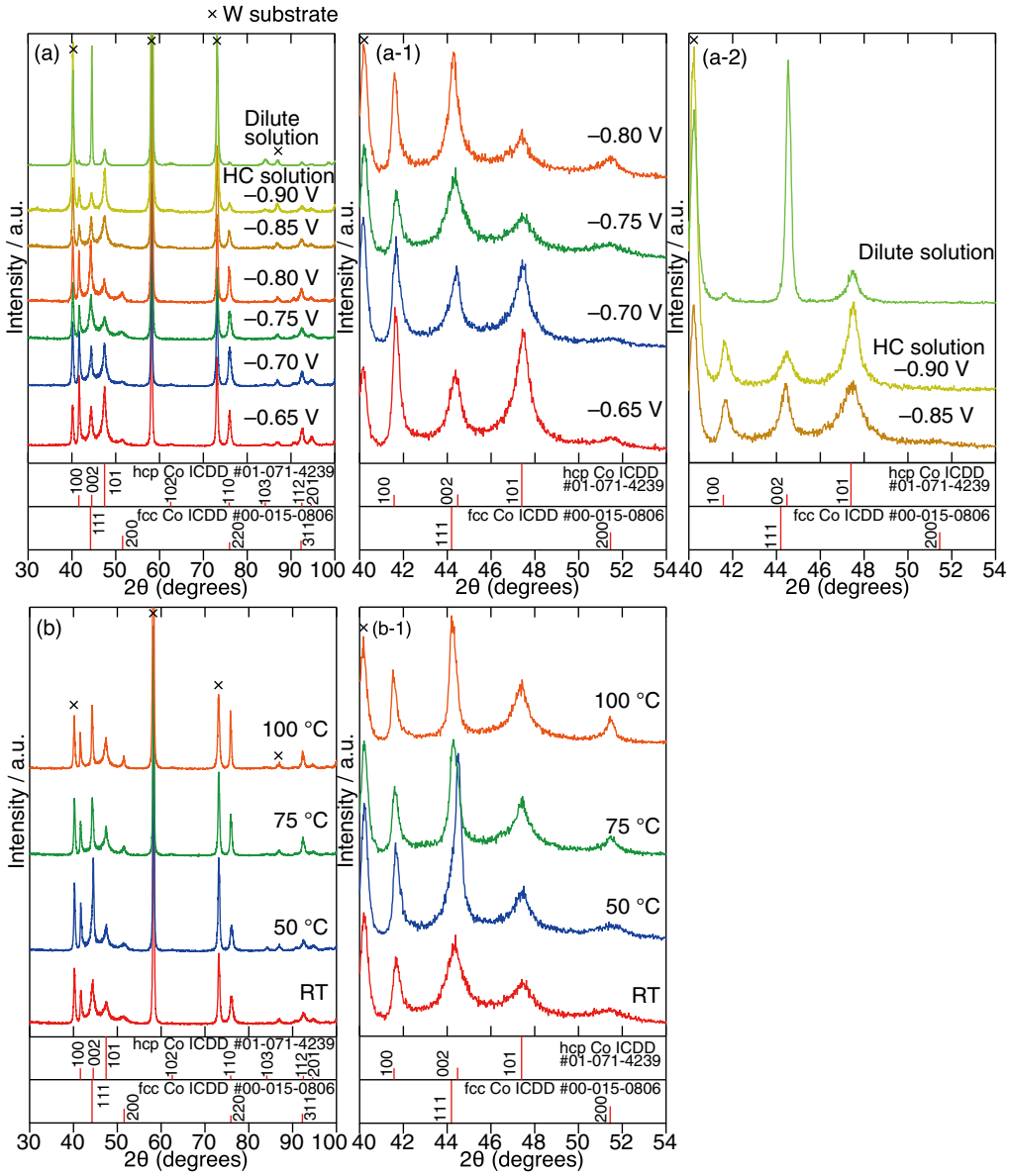

Fig. 3 XRD patterns of the cobalt electrodeposits obtained (a) at room temperature (RT) from HC ($n = 3$) and dilute solutions containing 0.3 mol dm^{-3} $CoCl_2$ and (b) at four different temperatures from HC solution ($n = 3$) containing 0.3 mol dm^{-3} $CoCl_2$. The electrodeposition from the HC solution ($n = 3$) was carried out at six potentials and RT. Electrodeposition from the dilute solution was performed at −0.4 V vs. immersion potential of Co at RT. The electrodeposition from the HC solution ($n = 3$) at 50, 75, and 100°C was carried out at −0.4 V vs. immersion potential of Co to each solution. Potential −0.4 V vs. immersion potential of Co from the HC solution at RT corresponds to −0.75 V vs. Ag/AgCl. Figures (a-1)/(a-2) and (b-1) are extended views of (a) and (b), respectively.

Table 3 XPS quantitative analysis results (in atomic %) for the electrodeposit at −0.75 V vs. Ag/AgCl from HC solution ($n = 3$) at room temperature.

Ar^+ etching time / s	Co	O	C	Li	Cl	$Co(OH)_2$	CoO, CoO_4	Co
0	27.3	51.7	20.6	ND	0.5	100	0	0
1500	93.8	2.9	3.3	ND	ND	1	0	99

electrodeposited Co obtained from the HC solution at room temperature, corresponds to hydrogen desorption from the interstitial lattice.[32] Peaks at around $T = 450$ K increased with decreasing solution temperature, and the XRD data showed that the angle of the diffraction peak corresponding to the hcp 100 reflection shifted to a higher angle side with decreasing solution temperature: 41.52° (100°C), 41.60° (75°C), and 41.64° (50°C and room temperature). This result shows that the lattice contraction was caused by hydrogen trapping in the monovacancies, i.e., the formation of vacancy-H clusters.[33,34] A similar hydrogen desorption peak from the monovacancy of hcp-Co was observed in the previous study.[32] A peak at $T = 700$ K was observed as a shoulder only for the electrodeposited Co obtained from the

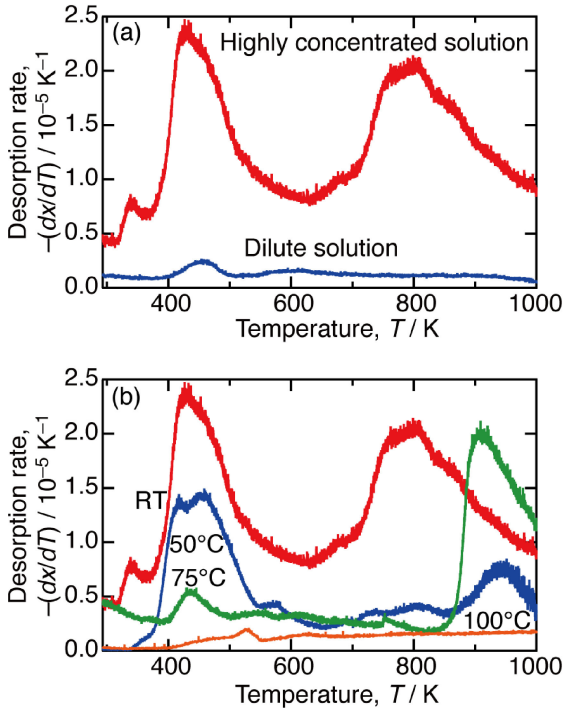

Fig. 4 TDS spectra of the cobalt electrodeposits obtained (a) from HC ($n = 3$) and dilute solutions containing 0.3 mol dm^{-3} $CoCl_2$ at room temperature (RT) and (b) from HC solution ($n = 3$) containing 0.3 mol dm^{-3} $CoCl_2$ at elevated temperatures.

HC solution at room temperature. This peak is believed to be hydrogen desorbed from the high-occupancy sites of fcc-Co.[32] A peak at around 800–880 K found in several spectra is considered to be the desorption of molecular hydrogen trapped at the grain boundaries and voids as the grains grew by recrystallization because the temperature range (700–900 K) of the peak corresponds to the recrystallization temperature of cobalt, which is 707 to 884 K (0.4 to 0.5 T_m), estimated from the melting point of Co ($T_m = 1768$ K). The integral width of the hcp 100 reflection was 0.39° for the Co electrodeposited at 50 and 75°C, whereas it was 0.42° for the Co obtained from the HC solutions at room temperature. This result shows improved crystallinity and that the crystallite size increases with increasing solution temperature. Therefore, in the Co electrodeposited at 50 and 75°C, grain growth by recrystallization and the concomitant hydrogen desorption start to be observed at approximately 880 K, a temperature that is higher than that of the electrodeposited Co obtained at room temperature. Note that the peak(s) at around 800–880 K was not observed for the Co treated at high temperatures[32] under high hydrogen pressure because it is assumed to be due to the good crystallinity and low grain boundary density of Co before recrystallization.[32]

Aside from the state of hydrogen, the total amount of hydrogen contained is more important in the context of the present study. For the deposits obtained at room temperature, the resulting hydrogen content represented by the H/Co atomic ratio was 9.2×10^{-3} for the cobalt electrodeposited from the HC solution and only 8.7×10^{-4} for that from the diluted solution. Specifically, approximately ten times more hydrogen was co-deposited with cobalt from the HC solution, despite the higher current efficiency; 99.3% in this case (see Table 2). If the remaining 0.7% of hydrogen were all incorporated into the cobalt, the H/Co ratio would be 14×10^{-3}. This value is close to the value of 9.2×10^{-3} determined by TDS analysis, indicating that most of the hydrogen reduced from the HC solution was captured in the cobalt without evolution as H_2 gas. The H/Co ratios for the cobalt obtained from HC solutions at elevated temperatures were 3.6×10^{-3} (50°C), 3.8×10^{-3} (75°C), and 8.5×10^{-4} (100°C), whereby the incorporated hydrogen tended to decrease with increasing deposition temperature.

All the above results indicate that hydrogen evolution is suppressed in a highly concentrated environment; however, for some reason, the ratio of hydrogen incorporation into cobalt is increased compared to that in dilute solutions. The suppression of hydrogen evolution does not imply the suppression of hydrogen uptake.

3.3 Relationship between hydrogen and the crystal phase of the electrodeposited cobalt

Nakahara *et al.* discussed the reason why the fcc phase co-deposits during cobalt electrodeposition from aqueous solutions, in relation to the formation of fcc Co-H alloys.[2] They explained that once electrodeposition is completed — since hydrogen diffuses quickly even at room temperature and the fcc phase is thermodynamically unstable at room temperature under ambient pressure — the fcc phase undergoes a phase transition to the hcp structure, partially retaining the fcc structure as stacking faults. In fact, in the electrodeposition of cobalt from dilute aqueous solutions in previous studies,[3,6–9] hydrogen evolution was frequently observed only when fcc-Co was co-deposited. Under such conditions with remarkable hydrogen evolution, electrodeposition proceeds with high hydrogen entrainment, which may result in the formation of Co-H alloys. Specifically, in these studies, hydrogen stabilized the fcc structure of the electrodeposited Co. Notably, under very high hydrogen pressure (>8 GPa), cobalt is also known to exhibit the fcc structure at room temperature.[32,35]

In this study, the TDS results revealed that the hydrogen content was higher in the cobalt electrodeposited from HC solution than that from dilute solution. In this case, the amount of hydrogen evolved should not be sufficient to form fcc-Co. Nevertheless, fcc-Co was co-deposited, and the H/Co was high at 9.2×10^{-3}. In addition, a previous study reported that cobalt electrodeposits from a dilute aqueous solution at 273 K under a constant current of 200 A m^{-2} and at 323 K under 100 A m^{-2} have H/Co ratios of 7.3×10^{-3} and 11.2×10^{-3}, respectively.[36] In both cases of the previous study,[36] only the hcp phase was obtained, while the hydrogen contents were not significantly different from those of the cobalt electrodeposited from the HC solution. In addition, the current efficiencies of cobalt electrodeposition in the cases of the previous study[36] are thought to be lower than those in the HC solutions. Thus, the fact that the crystal phase of the electrodeposited cobalt differs cannot be explained by the conventional way of thinking that hydrogen evolution produces fcc-Co.

The conventional way of thinking also cannot explain the co-deposition of fcc-Co electrodeposited at elevated temperatures such as 50, 75, and 100°C. At these temperatures, fcc-

Table 4 Integrated intensities and fcc fractions of the cobalt electrodeposits using the HC solution ($n = 3$) at 50, 75, 100°C, and room temperature (RT).

Temperature	fcc fraction / %	$I_{hcp\,100}$	$I_{hcp\,101}$	$I_{hcp\,002}/I_{fcc\,111}$	$I_{fcc\,111}$	$I_{hcp\,110}/I_{fcc\,220}$	$I_{fcc\,220}$	$I_{fcc\,200}$
RT	27	67	66	181	80	142	20	32
50 °C	21	92	92	309	80	112	20	32
75 °C	22	72	133	164	75	157	19	30
100 °C	28	72	115	154	91	158	23	36

Co electrodeposition still occurred, despite the lower hydrogen contents. It is probable that these low hydrogen contents are due to the high temperature, which allows hydrogen to diffuse and escape easily. Even so, if hydrogen stabilizes fcc-Co, the cobalt obtained from high-temperature solutions undergoes a phase transition to the hcp phase more readily than that obtained from the room-temperature solution.

To compare the volume fraction of fcc-Co in the electrodeposited cobalt films, we proceeded to estimate the volume fraction of fcc using eq. (1).

$$\text{fcc fraction } (\%) = \frac{I_{\text{fcc }111} + I_{\text{fcc }220} + I_{\text{fcc }200}}{I_{\text{hcp }100} + I_{\text{hcp }101} + I_{\text{hcp }002/\text{fcc }111} + I_{\text{hcp }110/\text{fcc }220} + I_{\text{fcc }200}} \quad (1)$$

where I values are the integrated intensities of the X-ray diffraction peaks. The results for the fcc fraction and I values are summarized in Table 4. Because we could not distinguish the 111 reflections of fcc from 002 of hcp and the 220 of fcc from 110 of hcp, $I_{fcc\,111}$ and $I_{fcc\,220}$ were calculated from the integrated intensity of $I_{fcc\,200}$ using ICDD PDF data (#00-015-0806)[37] assuming that fcc-Co is randomly oriented, where $I_{fcc\,111}$:$I_{fcc\,200} = 100$:40 and $I_{fcc\,220}$:$I_{fcc\,200} = 25$:40. The resulting fcc volume fractions are almost identical irrespective of the deposition temperature, suggesting that factor(s) other than hydrogen are responsible for fcc-Co formation during electrodeposition in HC solutions. Specific factors will be clarified in future studies. Note that the orientation of hcp-Co changes slightly with temperature, as shown by comparing the 100 and 101 reflections of hcp-Co (Table 4). Therefore, the orientation of the fcc phase may also have some temperature dependence and the above fcc fraction, calculated based on the assumption that fcc Co is randomly oriented, may be somewhat incorrect. However, because the XRD data do not show whether the fcc-Co is randomly oriented, we believe that the above method is the best method for estimating the fcc fraction from the diffraction peaks.

3.4 Discussion on the readiness of hydrogen co-deposition on cobalt from highly concentrated solutions

In general, irrespective of the current efficiency, the amount of hydrogen detected in metals electrodeposited in aqueous solutions is not large, except in the case of palladium which tends to form hydrides. This means that most of the hydrogen reduced during electrodeposition readily escapes from electrodeposits as H_2 bubbles. To incorporate hydrogen atoms into electrodeposits, it is important that the adsorbed hydrogen atoms do not escape as H_2 molecules before subsequent metal ions are reduced and deposited. Because our cobalt electrodeposition was performed in the potential range without the direct reduction of water, we discuss only the hydrogen evolution mechanism by proton reduction. Two primary hydrogen evolution mechanisms are known: the Volmer-Tafel and Volmer-Heyrovsky mechanisms.[38] In the Volmer-Tafel mechanism, protons on the metal are reduced to hydrogen atoms (Volmer step).

$$H^+ + e^- + M \rightarrow H\text{-}M \quad (2)$$

Two adsorbed hydrogen atoms then meet to form molecular hydrogen and subsequently desorb (Tafel step).

$$2H\text{-}M \rightarrow H_2 + 2M \quad (3)$$

In the Volmer-Heyrovsky mechanism, the proton is reduced on the adsorbed hydrogen atom according to reaction (4) to form molecular hydrogen (Heyrovsky step).

$$M\text{-}H + H^+ + e^- \rightarrow H_2 + M \quad (4)$$

Considering the hydrogen adsorption energy of cobalt, we can say that the Heyrovsky step is presumed to be the rate-limiting process of hydrogen evolution on cobalt.[39] Measurements of proton diffusion coefficients with RDEs (Fig. 2 and Table 1) showed that proton diffusion was very slow in our LiCl-based HC solution. In the HC solutions, it is reasonable to assume that such slow proton diffusion makes it difficult for the Heyrovsky mechanism to occur, that is, molecular hydrogen evolution is less likely to occur. If that is the case, the basically slow Tafel step on cobalt is the only remaining route for hydrogen evolution on it. However, the Tafel step has another problem: specific adsorption of anions. It is known that chloride (Cl^-) ions are specifically adsorbed on the surface of a number of metal cathodes.[40–42] Although the specific adsorption of Cl^- ions on cobalt surface has not been investigated well, we believe that the adsorption of Cl^- ions is likely to occur during electrodeposition, since cobalt has a high affinity for chlorine, as evidenced by its tendency to form chloride complexes in the oxidized state.[43,44] Note that the metals that have been investigated for the specific adsorption of Cl^- ions tend to form chloride complexes in their oxidized states.[45] In our electrodeposition using HC solution, the presence of highly active Cl^- ions

adsorbed on the growing cobalt surface may prevent the association of adsorbed hydrogen atoms with each other. As a result, the order of rate of reaction (2)–(4) is as follows: (2) slow, (4) very slow, and (3) extremely slow. In such situations, hydrogen atoms can be more readily incorporated into the growing metals despite the high current efficiency of metal deposition.

4. Conclusions

Cobalt electrodeposition was performed using a highly concentrated LiCl-based aqueous solution, which is expected to suppress hydrogen evolution. The current efficiency of cobalt deposition was more than 99% at potentials above −0.8 V, clearly indicating the suppression of hydrogen evolution. However, the TDS spectrum showed that the hydrogen content of cobalt obtained from the HC solution was one order of magnitude higher than that of cobalt obtained from the dilute aqueous solution. Furthermore, the electrodeposited cobalt obtained from the HC solutions was accompanied by the fcc phase. The co-deposition of fcc-Co occurred not only at room temperature, but also in solutions as high as 50, 75, and 100°C. It is believed that extensive hydrogen evolution during electrodeposition is necessary to obtain fcc-Co in conventional dilute aqueous solutions. However, in HC solutions, it was found that a large amount of hydrogen was not required to form fcc-Co. It was suggested that factors other than hydrogen were responsible for fcc-Co formation. We suggest that the reason for the hydrogen incorporation is that proton diffusion is very slow in HC solutions. Therefore, hydrogen atoms can be more readily incorporated into the cobalt electrodeposits despite the high current efficiency of cobalt deposition.

Acknowledgment

This work was financially supported by a Grant-in-Aid for Scientific Research (S) (Grant No. 20H05663; K. M.) from the Japan Society for the Promotion of Science (JSPS), a Grant-in-Aid for JSPS Fellows (Grant No. 22J15852; R. M.), and JST SPRING, Grant Number JPMJSP2110.

REFERENCES

1) T. Nishizawa and K. Ishida: Bull. Alloy Phase Diagr. **4** (1983) 390–395.
2) S. Nakahara and S. Mahajan: J. Electrochem. Soc. **127** (1980) 283–288.
3) A. Vicenzo and P.L. Cavallotti: Electrochim. Acta **49** (2004) 4079–4089.
4) C. Auth *et al.*: 2017 IEEE International Electron Devices Meeting (IEDM), (IEEE, 2017) pp. 29.1.1–29.1.4. doi:10.1109/IEDM.2017.8268472.
5) N. Bekiaris, Z. Wu, H. Ren, M. Naik, J.H. Park, M. Lee, T.H. Ha, W. Hou, J.R. Bakke, M. Gage, Y. Wang and J. Tang: 2017 IEEE International Interconnect Technology Conference (IITC), (IEEE, 2017) pp. 1–3. doi:10.1109/IITC-AMC.2017.7968981.
6) T. Cohen-Hyams, W.D. Kaplan and J. Yahalom: Electrochem. Solid-State Lett. **5** (2002) C75–C78.
7) J. Goddard and J.G. Wright: Br. J. Appl. Phys. **15** (1964) 807–814.
8) E. Gómez and E. Vallés: J. Appl. Electrochem. **32** (2002) 693–700.
9) S. Ali and M. Salim: Asian J. Chem. **25** (2013) 4137–4140.
10) D.R. Gabe: J. Appl. Electrochem. **27** (1997) 908–915.
11) R. Fukui, Y. Katayama and T. Miura: Electrochemistry **73** (2005) 567–569.
12) M. Li, Z. Wang and R.G. Reddy: Electrochim. Acta **123** (2014) 325–331.
13) T. Le Manh, E.M. Arce-Estrada, I. Mejía-Caballero, J. Aldana-González, M. Romero-Romo and M. Palomar-Pardavé: J. Electrochem. Soc. **165** (2018) D285–D290.
14) L. Suo, O. Borodin, T. Gao, M. Olguin, J. Ho, X. Fan, C. Luo, C. Wang and K. Xu: Science **350** (2015) 938–943.
15) Y. Yamada, K. Usui, K. Sodeyama, S. Ko, Y. Tateyama and A. Yamada: Nat. Energy **1** (2016) 16129.
16) M. McEldrew, Z.A.H. Goodwin, S. Bi, A.A. Kornyshev and M.Z. Bazant: J. Electrochem. Soc. **168** (2021) 050514.
17) A.A. Chialvo and J.M. Simonson: J. Chem. Phys. **119** (2003) 8052–8061.
18) J.A. Rard and S.L. Clegg: J. Chem. Eng. Data **42** (1997) 819–849.
19) L. Chen *et al.*: ACS Energy Lett. **5** (2020) 968–974.
20) L. Suo, O. Borodin, W. Sun, X. Fan, C. Yang, F. Wang, T. Gao, Z. Ma, M. Schroeder, A. von Cresce, S.M. Russell, M. Armand, A. Angell, K. Xu and C. Wang: Angew. Chem. Int. Ed. **55** (2016) 7136–7141.
21) N. Kadam and A. Sarkar: J. Energy Storage **54** (2022) 105265.
22) C.-Y. Chen, K. Matsumoto, K. Kubota, R. Hagiwara and Q. Xu: Adv. Energy Mater. **9** (2019) 1900196.
23) Q. Huang and T.W. Lyons: Electrochem. Commun. **93** (2018) 53–56.
24) M. Miyamoto, A. Kitada, K. Adachi, K. Fukami and K. Murase: J. MMIJ **137** (2021) 103–109.
25) K. Adachi, A. Kitada, K. Fukami and K. Murase: Electrochim. Acta **338** (2020) 135873.
26) N. Fukumuro, K. Tohda and S. Yae: J. Electrochem. Soc. **169** (2022) 122505.
27) D.R. Lide: *CRC Handbook of Chemistry and Physics 84th Edition*, (CRC PRESS, Boca Raton, 2004) pp. 5-93–5-95.
28) S. De, J. White, T. Brusuelas, C. Patton, A. Koh and Q. Huang: Electrochim. Acta **338** (2020) 135852.
29) M. Takahashi: Corros. Eng. **23** (1974) 625–637.
30) J. Dille, J. Charlier and R. Winand: J. Mater. Sci. **32** (1997) 2637–2646.
31) R. Sard, C.D. Schwartz and R. Weil: J. Electrochem. Soc. **113** (1966) 424–428.
32) Y. Fukai, S. Yokota and J. Yanagawa: J. Alloy. Compd. **407** (2006) 16–24.
33) Y. Fukai and N. Ōkuma: Jpn. J. Appl. Phys. **32** (1993) L1256–L1259.
34) Y. Fukai and N. Ōkuma: Phys. Rev. Lett. **73** (1994) 1640–1643.
35) V.E. Antonov, T.E. Antonova, M. Baier, G. Grosse and F.E. Wagner: J. Alloy. Compd. **239** (1996) 198–202.
36) A. Nakayama, N. Fukumuro, S. Yae and H. Matsuda: ECS Trans. **25**(34) (2010) 79–85.
37) H.E. Swanson, M.C. Morris and E.H. Evans: Natl. Bur. Stand. U.S. Monogr. **25**(4) (1966) 10.
38) V.S. Bagotsky: *Fundamentals of Electrochemistry, Second Edition*, (John Wiley & Sons, New York, 2006) pp. 261–295.
39) J.K. Nørskov, T. Bligaard, A. Logadottir, J.R. Kitchin, J.G. Chen, S. Pandelov and U. Stimming: J. Electrochem. Soc. **152** (2005) J23–J26.
40) D.C. Grahame and B.A. Soderberg: J. Chem. Phys. **22** (1954) 449–460.
41) K. Lust, M. Väärtnõu and E. Lust: Electrochim. Acta **45** (2000) 3543–3554.
42) J.O'M. Bockris, R.E. White and B.E. Conway: *Modern Aspects of Electrochemistry*, No. 31, (Plenum Press, New York, 1997) pp. 181–250.
43) K. Kim, D. Raymond, R. Candeago and X. Su: Nat. Commun. **12** (2021) 6554.
44) N.H. Chung, Y.G. Wu and M. Tabata: Anal. Sci. **21** (2005) 1287–1290.
45) R.M. Smith and A.E. Martell: *Critical Stability Constants Vol. 4 Inorganic Complexes*, (Plenum Press, New York, 1976) pp. 104–112.